A broad specificity β-propeller enzyme from *Rhodopseudomonas palustris* that hydrolyzes many lactones including γ-valerolactone

Benjamin W. Hall[1,2,3] , Craig A. Bingman[2,4], Brian G. Fox[2,4], Daniel R. Noguera[2,3,5] , and Timothy J. Donohue[2,3,6,*]

From the [1]Laboratory of Genetics, University of Wisconsin–Madison, Madison, Wisconsin, USA; [2]Department of Energy Great Lakes Bioenergy Research Center, Madison, Wisconsin, USA; [3]Wisconsin Energy Institute, University of Wisconsin–Madison, Madison, Wisconsin, USA; [4]Department of Biochemistry, [5]Department of Civil and Environmental Engineering, and [6]Department of Bacteriology, University of Wisconsin–Madison, Madison, Wisconsin, USA

Edited by Joseph Jez

Lactones are prevalent in biological and industrial settings, yet there is a lack of information regarding enzymes used to metabolize these compounds. One compound, γ-valerolactone (GVL), is used as a solvent to dissolve plant cell walls into sugars and aromatic molecules for subsequent microbial conversion to fuels and chemicals. Despite the promise of GVL as a renewable solvent for biomass deconstruction, residual GVL can be toxic to microbial fermentation. Here, we identified a Ca^{2+}-dependent enzyme from *Rhodopseudomonas palustris* (Rpa3624) and showed that it can hydrolyze aliphatic and aromatic lactones and esters, including GVL. Maximum-likelihood phylogenetic analysis of other related lactonases with experimentally determined substrate preferences shows that Rpa3624 separates by sequence motifs into a subclade with preference for hydrophobic substrates. Additionally, we solved crystal structures of this β-propeller enzyme separately with either phosphate, an inhibitor, or a mixture of GVL and products to define an active site where calcium-bound water and calcium-bound aspartic and glutamic acid residues make close contact with substrate and product. Our kinetic characterization of WT and mutant enzymes combined with structural insights inform a reaction mechanism that centers around activation of a calcium-bound water molecule promoted by general base catalysis and close contacts with substrate and a potential intermediate. Similarity of Rpa3624 with other β-propeller lactonases suggests this mechanism may be relevant for other members of this emerging class of versatile catalysts.

Lactones are a diverse set of cyclic ester-containing compounds that play many roles in chemical and biological systems. Naturally occurring lactones function as metabolic intermediates (1–4), signaling molecules (5–7), antibiotics (8, 9), and more. In addition, many animals, plants, and ecosystems are exposed to xenobiotic lactones produced by industry. γ-valerolactone (GVL) is one such lactone used as a solvent that can be both produced from plant biomass and used to dissolve plant cell walls into sugars and aromatic molecules for subsequent microbial conversion to fuels and chemicals (10, 11). Despite the prevalence of lactones in biology and the promise of GVL as a renewable solvent for biomass deconstruction, basic information on the enzymes used to metabolize these compounds is incomplete. Moreover, there are bottlenecks associated with the potential use of GVL for bioenergy purposes. For example, even after the majority is removed from the dissolved biomass (10), the residual GVL can be toxic to microbial fermentation (12). Alternatively, residual GVL could also represent a significant carbon and energy source for tolerant microbes that could assimilate this lactone or convert it into other valuable products. Thus, the use of GVL as a renewable solvent for plant deconstruction would benefit from the identification of microbial enzymes that can hydrolyze the lactone ring of this compound.

Among the enzymes that have been shown to hydrolyze lactones, the best characterized are the homoserine lactonases such as AiiA from *Bacillus* spp., which hydrolyze the *N*-acyl homoserine lactones used as quorum sensing molecules by some Gram-negative bacteria (13, 14). Other bacterial lactonases have been identified that hydrolyze aromatic lactones (15, 16), sugar lactones (17–21), and lactones with different ring sizes (22). In addition, the human enzyme paraoxonase 1 (PON1) has been shown to hydrolyze many naturally occurring and xenobiotic lactones (23, 24).

Earlier, the α-proteobacterium *Rhodopseudomonas palustris* was reported to use GVL as a sole organic carbon source (25). Here, a Ca^{2+}-dependent enzyme from this microbe, encoded by *rpa3624*, is shown to hydrolyze aliphatic and aromatic lactones and esters, including GVL. We compare its crystal structure and other properties to other reported lactonases and propose reannotation of *rpa3624* to better reflect its substrate specificity.

Results

R. palustris *Rpa3624 has lactonase activity with GVL*

The alpha-proteobacterium *R. palustris* CGA009 removed GVL from culture medium faster than the reported rate of its

---

* For correspondence: Timothy J. Donohue, tdonohue@bact.wisc.edu.

spontaneous hydrolysis in aqueous solutions (11, 25), suggesting that GVL hydrolysis was enzymatically catalyzed. To test this, *R. palustris* whole cell extracts were added to solutions of GVL, and HPLC-MS/MS was used to quantify GVL and its predicted hydrolysis product, 4-hydroxyvalerate (4-HV). These experiments showed that GVL was stoichiometrically converted to 4-HV in the presence of an *R. palustris* whole cell extract (Fig. 1). Thus, *R. palustris* contains one or more enzymes able to hydrolyze the GVL lactone ring.

To identify candidate enzymes able to catalyze GVL hydrolysis, we analyzed the *R. palustris* CGA009 genome for homologs of enzymes that were known or predicted to cleave lactones. *R. palustris* CGA009 has two genes that encode homologs of the *Bacillus thuringiensis* AiiA enzyme that hydrolyzes γ-lactones (26), *rpa4424* and *rpa2488*, and four other genes predicted to encode proteins with similar metallo-β-lactamase domains, *rpa0798*, *rpa1095*, *rpa2779*, and *rpa4673*. In addition, PSI-BLAST was used to build a Position Specific Score Matrix for PON1, a human enzyme shown to hydrolyze GVL (23, 27). Using this PSSM for PON1 in a PSI-BLAST against the *R. palustris* CGA009 genome returned *rpa3624*, an annotated gluconolactonase, as the only gene with a significant alignment (E < 0.005). Expression constructs were created for each of these seven candidate lactonases as described in Experimental Procedures, and an *Escherichia coli* transformant expressing the His-tagged version of Rpa3624 was the only one to show GVL hydrolysis activity in cell-free extracts (Table S1).

Lactonase activity of R. palustris Rpa3624 with GVL and other lactone substrates

Purified Rpa3624 was tested for activity with GVL and a set of other chemically or structurally related substrates. Using identical assay conditions, Rpa3624 had measurable activity with γ-, δ-, and ε-lactones as well as some esters (Table 1), but no measurable activity with gluconolactone or N-acyl
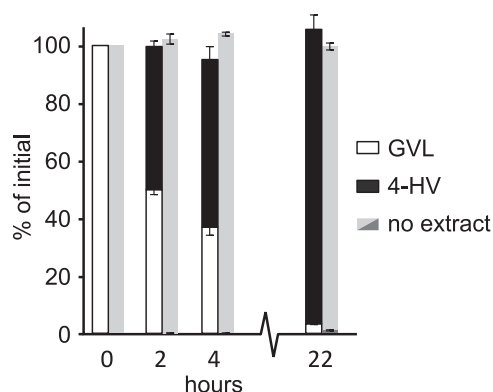
homoserine lactones. Rpa3624 shows pronounced differences in substrate preference as measured by k_{cat}/K_M values. The apparent K_M values for the tested substrates ranged over two orders of magnitude, while k_{cat} values differed by ∼10-fold, aside from the low k_{cat} observed with octyl acetate, a non-lactone substrate. Substrates with shorter aliphatic chains had higher K_M values; for example, the K_M values of γ-butyrolactone and GVL exceeded 600 mM. Still, these higher K_M substrates have similar turnover numbers compared to other compounds that are hydrolyzed by Rpa3624. These data suggest that the difference in substrate preference reflects differences in K_M rather than k_{cat}.

The lack of enzyme activity with gluconolactone was not anticipated, as *rpa3624* is annotated to be a gluconolactonase (Table S1). Although the related enzyme human PON1 is also annotated to contain a gluconolactonase domain, this enzyme also lacks detectable activity with sugar lactones (4, 28). Thus, we sought to determine if primary sequence could distinguish between enzymes that hydrolyze sugar lactones *versus* enzymes like Rpa3624 that hydrolyze the lactone ring of more hydrophobic substrates. A maximum-likelihood phylogenetic tree created from lactonases with evidence for substrate preference split into two branches corresponding to substrate preference, except for the placement of XC5397 and ZMO1649 (Fig. 2). This tree predicts that Rpa3624 and other enzymes with activity on hydrophobic lactones are more closely related to each other than to known sugar lactonases. Notably, this grouping is not driven by phylogenetic relationships between the organisms, as the sugar and hydrophobic lactonase groupings containing sequences from both prokaryotes and eukaryotes. From this data, it appears that a properly assembled list of primary sequences can yield motifs diagnostic for either sugar or hydrophobic lactonase types such as Rpa3624.

Rpa3624 is a dimeric β-propeller enzyme

The 3-dimensional crystal structure of Rpa3624 was solved at a resolution of 1.72 Å by anomalous diffraction from a holmium-derivatized crystal (Fig. 3; PDB 7RIS). Refinement statistics for this structure and others (see below) are shown in Table 2.

In this structure, Rpa3624 adopts a six-bladed β-propeller fold, with a calcium ion, a sodium ion, and a phosphate ion present at full occupancy (Fig. 3). The calcium and phosphate ions interact at the top of a central channel, while the sodium ion sits about midway through the channel. Nine residues located near the calcium and phosphate ions (numbers 75–83) and another four residues on the outer surface of the β-propeller (numbers 209–212) had no defined electron density. The calcium ion makes direct contacts with carboxylate groups of residues E15 and D229, the amide groups of N123 and N172, the hydroxyl group of S230, one oxygen of the phosphate ion, and a water (HOH5). The average bond length for these interactions is 2.4 Å. The sodium ion (Fig. S1) has octahedral coordination from the carbonyl backbone atoms from L231, N271, and I272, and

Figure 1. Time-dependent conversion of GVL (*white bars*) to 4-HV (*black bars*) using a whole cell extract from *Rhodopseudomonas palustris*. Data from samples in the presence of cell extract are included in the left column in each pair, while GVL data from control assays (*gray bars*) lacking any added cell extract are shown as the right column in each pair. Error bars represent SD of three technical replicates. 4-HV, 4-hydroxyvalerate; GVL, γ-valerolactone.

Table 1

Kinetic parameters for reaction of Rpa3624 with various substrates

Compound	Structure	k_{cat} (s^{-1}) (95% CI)	K_M (mM) (95% CI)	k_{cat}/K_M (s^{-1} M^{-1})
γ-butyrolactone[a,b]		>70	>600	1.18×10^2
γ-valerolactone[a,b]		>326	>500	6.73×10^2
γ-decanolactone		135 (107–180)	2.36 (1.15–4.82)	5.72×10^4
δ-valerolactone		754 (621–946)	74.0 (40.7–133)	1.02×10^4
δ-nonalactone[a]		266 (175–591)	21.9 (11.4–60.4)	1.21×10^4
Dihydrocoumarin		308 (241–438)	1.85 (0.976–3.77)	1.66×10^5
ε-caprolactone		110 (72.8–304)	181 (48.0–1080)	6.08×10^2
Octyl acetate[a]		0.167 (0.0966–2.95)	1.25 (0.291–42.8)	1.34×10^2
Phenyl acetate[a,b]		>38.6	>12.5	3.19×10^3
Ethyl acetate		ND, <1.1	ND, >150	ND, <7.3
Coumarin		ND, <0.048	ND, >20	ND, <2.4
Mevalonolactone		ND, <3.2	ND, >50	ND, <64
D-gluconolactone		ND, <0.32	ND, >10	ND, <32
p-coumaryl homoserine lactone		ND, <0.39	ND, >5	ND, <78
3-oxo-hexanoyl homoserine lactone		ND, <0.11	ND, >10	ND, <11

No activity detected so the limit of detection is reported. For rate measurements, the limit of detection is 2× the rate of spontaneous hydrolysis of the substrate.
Abbreviation: ND, not detected.
[a] Substrate did not yield saturation kinetics behavior, perhaps due to solubility issues.
[b] Data were better fit with a linear model than the Michaelis-Menten equation (F test, $p > 0.05$), so the highest activity values and substrate concentrations are reported and estimates of k_{cat}/K_M are calculated from a linear fit of the data points.

HOH19, HOH22, and HOH33 with an average bond length of 2.5 Å. The coordinating waters reside in a large internal cavity in the protein.

The unit cell for these Rpa3624 crystals contains one polypeptide. However, polypeptides in neighboring unit cells form an extensive dimer interface of about one thousand Å^2.

Size-exclusion chromatography using three separate protein samples also showed that purified Rpa3624 eluted at a predicted molecular weight (MW) of 58.1 kDa, approximately twice the calculated MW of a monomer (32.8 kDa) (Fig. S2). Moreover, the protein interface predictor PDBePISA (29) (http://www.ebi.ac.uk/pdbe/prot_int/pistart.html) predicts a

ASBMB

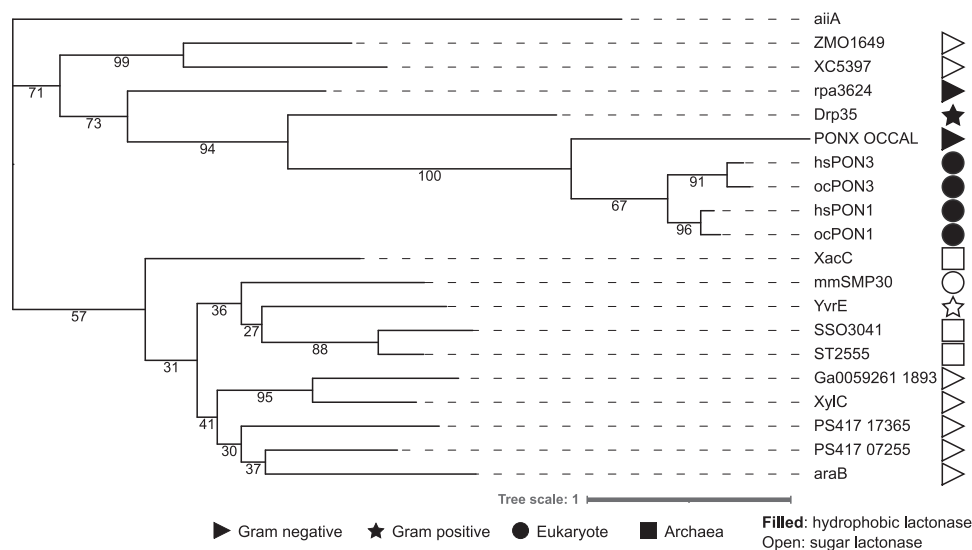*J. Biol. Chem.* (2023) 299(1) 102782 **3**

Figure 2. Hydrophobic lactonases are more related to each other than to sugar lactonases. This maximum likelihood tree was built using Rpa3624-related lactonases and AiiA as an outgroup to root the tree. The legend for symbols is shown at the *bottom* of the figure. Bootstrap values for each node are shown. Details and references for each lactonase can be found in Table S2. This figure was created using Interactive Tree of Life (84).

protein-protein interface that matches the one observed in the crystal structure between neighboring unit cells. These analyses support the conclusion that the crystallographic dimer recapitulates features of the soluble protein.

Contributions of Ca²⁺ and phosphate to Rpa3624 lactonase activity

Many characterized lactonases require at least one metal ion for catalysis (30), so the calcium ion seen in the Rpa3624 crystal structure may have a role in catalysis. To independently test for the presence of the calcium in purified Rpa3624, inductively coupled plasma mass spectrometry (ICP-MS) showed that enzyme expressed and purified in media either lacking or containing 1 mM $CaCl_2$ contained 1.00 ± 0.05 equivalents of calcium (Table 3, n = 5 biological replicates). Magnesium and other metals analyzed were present at less than 0.05 eq, except for nickel, which was present at 0.5 ± 0.4 eq, presumably as carry-over from nickel-affinity purification of the recombinant Rpa3624 protein (Table S3).

To test the role of calcium in catalysis by Rpa3624, hydrolysis of the high-affinity lactone dihydrocoumarin (Table 1) was measured in the absence and presence of EGTA, a chelator more specific for calcium than EDTA (31). Incubation of Rpa3624 for 4 h at 30 °C in the presence of 10 mM EGTA decreased V_{max} by ~90%. Thus, calcium is required for Rpa3624 activity.

The role of the phosphate ion bound to calcium was also of interest. Rpa3624 was purified from cells grown in standard autoinduction medium (50 mM K_2HPO_4) and in medium that contained low K_2HPO_4 (1.32 mM). ICP-MS analysis of Rpa3624 purified from cultures grown in either the high- or low-phosphate media showed an average of 1.1 ± 0.8 (n = 3) and 1.5 ± 0.2 (n = 2) eq of phosphorus per monomer, respectively. Thus, decreasing phosphate in the growth medium did not decrease phosphate occupancy in Rpa3624. To test if the presence of phosphate had any impact on Rpa3624 activity, an additional 5, 50, or 300 mM NaH_2PO_4 (pH 8) was added to assay buffers that lacked
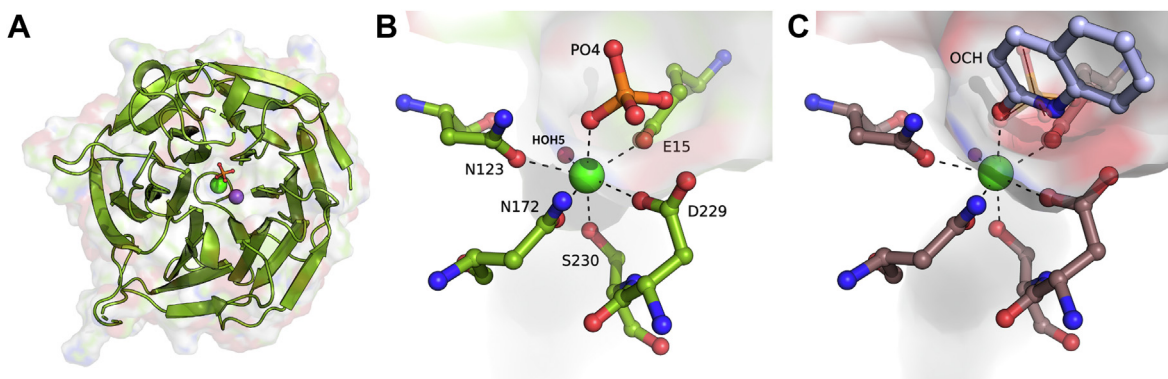

Figure 3. Crystal structure of phosphate-bound Rpa3624 (PDB 7RIS). *A,* the *top* view shows the six blades of the β-propeller, the phosphate molecule (*central orange and red sticks*) bound to the calcium (*green sphere*), and the sodium ion (*purple sphere*). *B,* the close-up view of the calcium coordination sphere shows the contacts holding the calcium ion in place. *C,* Rpa3624 crystallized in the presence of 2-HQ (*lavender,* PDB 7RIZ) shows that the carbonyl oxygen of 2-HQ overlaps with one of the phosphate oxygens in the phosphate-bound structure. 2-HQ, 2-hydroxyquinoline.

Table 2
Refinement statistics for the Rpa3624 crystal structures

PDB ID (ligand bound to calcium)	7RIS (Phosphate)	7RIZ (2-HQ)	8DJF (intermediate)	8DJZ (product)	8DK0 (substrate)
Wavelength	1.033	1.127	0.9787	0.9787	0.9787
Resolution range	35.74–1.72 (1.782–1.72)	33.19–1.71 (1.771–1.71)	38.03–1.553 (1.608–1.553)	38.03–1.553 (1.608–1.553)	38.03–1.553 (1.608–1.553)
Space group	P 32 2 1	P 32 2 1	P 32 2 1	P 32 2 1	P 32 2 1
Unit cell	a = b = 44.54 c = 189.95	a = b = 48.56 c = 199.12	a = b = 47.51 c = 199.02	a = b = 47.51 c = 199.02	a = b = 47.51 c = 199.02
Total reflections	477,422 (48,829)	596,379 (60,205)	404,681 (39,752)	404,681 (39,752)	404,681 (39,752)
Unique reflections	24,269 (2381)	30,590 (2983)	38,765 (3762)	38,765 (3762)	38,765 (3762)
Multiplicity	19.7 (20.5)	19.5 (20.2)	10.4 (10.6)	10.4 (10.6)	10.4 (10.6)
Completeness (%)	99.62 (99.29)	99.31 (98.19)	99.42 (98.81)	99.42 (98.81)	99.42 (98.81)
Mean I/sigma(I)	20.07 (1.72)	17.31 (1.65)	13.95 (1.17)	13.95 (1.17)	13.95 (1.17)
Wilson B-factor	27.94	27.55	25.47	25.47	25.47
R-merge	0.08686 (1.473)	0.1008 (1.421)	0.07998 (2.819)	0.07998 (2.819)	0.07998 (2.819)
R-meas	0.08923 (1.511)	0.1036 (1.458)	0.08441 (2.962)	0.08441 (2.962)	0.08441 (2.962)
R-pim	0.02012 (0.3297)	0.02366 (0.323)	0.02652 (0.8997)	0.02652 (0.8997)	0.02652 (0.8997)
CC1/2	1 (0.916)	0.999 (0.964)	0.999 (0.686)	0.999 (0.686)	0.999 (0.686)
CC*	1 (0.978)	1 (0.991)	1 (0.902)	1 (0.902)	1 (0.902)
Reflections used in refinement	24,193 (2367)	30,411 (2937)	38,669 (3748)	38,669 (3748)	38,669 (3748)
Reflections used for R-free	1996 (195)	1987 (192)	2998 (289)	2998 (289)	2998 (289)
R-work	0.177 (0.272)	0.177 (0.319)	0.178 (0.328)	0.180 (0.332)	0.176 (0.325)
R-free	0.200 (0.331)	0.209 (0.350)	0.211 (0.324)	0.212 (0.323)	0.211 (0.326)
CC(work)	0.964 (0.937)	0.972 (0.921)	0.968 (0.855)	0.968 (0.851)	0.970 (0.851)
CC(free)	0.969 (0.842)	0.965 (0.820)	0.965 (0.813)	0.965 (0.813)	0.966 (0.798)
Number of nonhydrogen atoms	2311	2511	2339	2339	2339
Macro-molecules	2190	2296	2205	2205	2205
Ligands	7	20	20	19	17
Solvent	114	202	124	124	125
Protein residues	293	306	293	293	293
RMS(bonds)	0.004	0.012	0.010	0.007	0.010
RMS(angles)	0.71	1.03	1.06	0.87	1.07
Ramachandran favored (%)	94.77	96.05	96.52	96.52	96.52
Ramachandran allowed (%)	5.23	3.95	3.48	3.48	3.48
Ramachandran outliers (%)	0.00	0.00	0.00	0.00	0.00
Rotamer outliers (%)	0.87	1.24	0.86	0.86	0.86
Clashscore	1.15	1.53	1.36	1.36	2.27
Average B-factor	38.13	37.04	37.69	37.61	39.18
Macro-molecules	38.17	36.75	37.65	37.55	39.12
Ligands	29.14	40.47	40.66	41.36	57.43
Solvent	37.84	40.09	38.18	38.45	38.98
Number of TLS groups	4	3	2	2	2
RSCC overall	0.879	0.881	0.871	0.869	0.871
RSCC ligand	0.989	0.904	0.844	0.809	0.756

CC* is a measure related to the protein model.

added calcium, and no inhibition or enhancement of dihydrocoumarin hydrolysis was observed (Fig. 4). Furthermore, ^{31}P-NMR of Rpa3624 suggested that the substrate analog 2-hydroxyquinoline (2-HQ, see below) displaced Rpa3624-bound phosphate (Fig. S3). Thus, the phosphate bound to calcium observed in the Rpa3624 crystal structure is likely displaced by substrate binding and thus neither plays a role in nor inhibits catalysis.

pH dependence of Rpa3624 activity

In other studied lactonases, the initial steps of catalysis are proposed to involve deprotonation of a water molecule by an

Table 3
Kinetic parameters determined for Rpa3624 substitution mutants using dihydrocoumarin as substrate

Mutant	Calcium content	k_{cat} (s⁻¹) (95% CI)	K_M (mM) (95% CI)	k_{cat}/K_M (s⁻¹ M⁻¹)	Catalytic efficiency (% of WT)
WT	1.00 ± 0.05	336 (246–551)	2.6 (1.3–6.1)	1.3×10^5	100%
E15Q	0.01	ND, <0.080	ND, >16	ND, <5	ND, <0.004%
E15D[a]	0.70	>62	>16	4.0×10^3	3.1%
N123D[a]	0.82	>2.4	>16	1.5×10^2	0.1%
N172A	No soluble protein				N/A
N172D[a]	0.83	>14	>16	6.6×10^2	0.5%
D229N	0.01	ND, <0.066	ND, >16	ND, <4.1	ND, <0.004%
D229E	0.31	ND, <0.81	ND, >16	ND, <51	ND, <0.04%

For rate measurements, the limit of detection is 2× the rate of spontaneous hydrolysis of the substrate.
Abbreviation: ND, not detected.
[a] Substrate did not yield saturation kinetics behavior, perhaps due to solubility issues, and data were better fit with a linear model than the Michaelis-Menten equation (F test, $p > 0.05$), so the highest activity values and substrate concentrations are reported and estimates of k_{cat}/K_M are calculated from a linear fit of the data points.
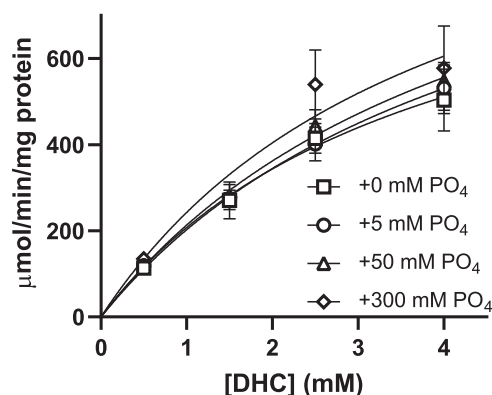
Figure 4. The presence of phosphate has minimal impact on Rpa3624-catalyzed hydrolysis of dihydrocoumarin. Error bars represent SD of three biological replicates.

acidic or basic side chain in the active site to form a hydroxyl ion that attacks the carbonyl carbon of the ester bond in the substrate, leading to hydrolysis of the lactone ring (15, 32, 33). To gain insights into the chemical nature of amino acid side chains that are important for catalysis by Rpa3624, the pH dependence of dihydrocoumarin hydrolysis was determined. Rpa3624 shows highest catalytic efficiency when assayed between pH 6 to 7 and retains activity in the pH range from 7 to 9 (Fig. 5). However, at pH 5.5 and below, catalytic efficiency dropped dramatically, apparently due to decreased k_{cat} values (Fig. S4). This pH-dependent decrease suggests that a deprotonated acidic amino acid in the vicinity of the active site may participate in catalysis (either E15 or D229, see below).

Activity of Rpa3624 substitution mutants

To investigate the potential roles of active site amino acid side chains in Rpa3624 activity, single amino acids in the proximity of the calcium ion were mutated (E15Q, E15D, N123D, N172A, N172D, D229N, D229E), and soluble recombinant protein was purified for each except N172A, which was insoluble when expressed in *E. coli*. Each of the soluble variant enzymes showed undetectable or greatly reduced catalytic efficiency (Table 3). While the N to D (N123D and N172D) and E15D mutations gave variant enzymes that
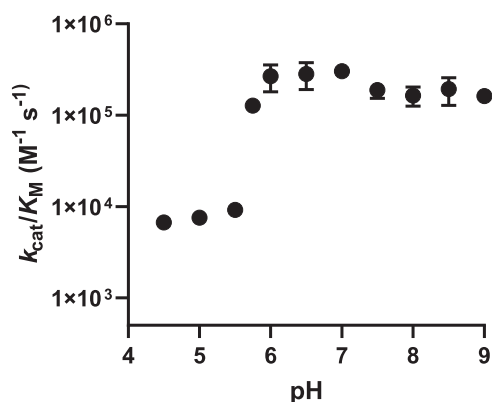

Figure 5. Catalytic efficiency of Rpa3624 measured as a function of pH. Dihydrocoumarin was used as the substrate (mean ± SD, *n* = 3 biological replicates). Error bars are not shown when they would be smaller than the symbol.

retained some activity with dihydrocoumarin, the acid to amide mutations (E15Q and D229N) and D229E gave variant enzymes with no detectable activity. Since calcium binding is important for activity (see above), all variant enzymes were analyzed for their ability to bind calcium using ICP-MS (Table 3). Even for enzymes that retained some activity, calcium occupancy was reduced by 20 to 30% (E15D, N123D, N172D). No calcium was detected in the E15Q and D229N variant enzymes that lacked activity. Interestingly, the D229E variant enzyme retained significant calcium binding but showed no detectable activity in the presence of dihydrocoumarin. These results indicate the importance of maintaining charge balance to support calcium binding in the active site and also suggest that D229 may have an additional, spatially defined role in catalysis.

Interaction of Rpa3624 with the lactonase inhibitor 2-HQ

2-HQ, a nonhydrolyzable analog of dihydrocoumarin, is a potent inhibitor of the related lactonase PON1 (23). Assays of dihydrocoumarin hydrolysis showed that 2-HQ was also an inhibitor of Rpa3624 activity when present at 2 to 8 mM (Fig. S5). The structure of Rpa3624 bound to 2-HQ was also solved (Table 2 and Fig. 3*C*), and the 2-HQ–bound enzyme has similar features to the phosphate-bound enzyme (RMSD of 0.26 Å), including no changes in the positions of calcium-binding residues or HOH5 bound to calcium. However, the 2-HQ–bound crystal gave defined electron density for residues 77 to 82 and 209 to 212, which could not be modeled in the phosphate-bound structure. The carbonyl oxygen of 2-HQ is bound to the calcium ion (2.5 Å) and occupies the same position as an oxygen from phosphate in the phosphate-bound structure (shown as transparent *orange* sticks in Fig. 3*C*). The nitrogen of 2-HQ hydrogen bonds with the carboxylate of residue D229 (1.9 Å) and the distal portion of 2-HQ makes contacts with residue M83 of the same monomer and Y211 from the other subunit in the Rpa3624 dimer.

Interaction of Rpa3624 with GVL

The structure of Rpa3624 was also solved in the presence of 20% GVL (Table 2 and Fig. 6), which is both an enzyme substrate and a cryoprotecting solvent miscible with water. Preformed Rpa3624 crystals were soaked with either *S*-GVL or *R*-GVL to explore whether the enzyme would exhibit stereochemical preference for binding. Analysis of multiple crystals from both stereoisomer soaks yielded electron density in the active site near to calcium as observed in other lactonases (15, 28, 34), but the diffraction data were better quality from crystals soaked with *S*-GVL than *R*-GVL, so the former were used for analysis.

The electron density in the predicted active site of the GVL-soaked Rpa3624 crystals does not match unambiguously with the expected density of either a GVL molecule (Fig. 6*A*, SGV; PDB 8DK0), a predicted tetrahedral reaction intermediate (Fig. 6*B*, 4R4; PDB 8DJF), or the hydrolysis product (Fig. 6*C*, 4HV; PDB 8DJZ). Thus, it is possible that the crystals contain a mixture of GVL, possibly in two different conformations
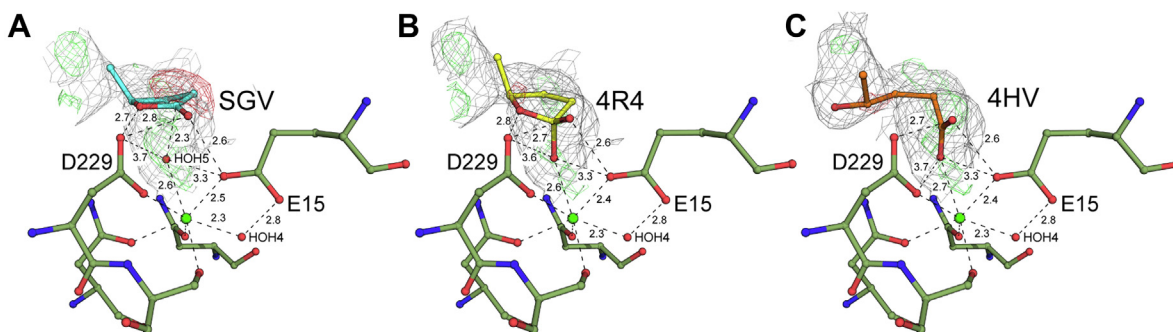
Figure 6. Comparison of electron density with models of substrate, intermediate and product bound to Rpa3624. *A*, the substrate *S*-GVL; *B*, a putative tetrahedral intermediate; or *C*, the product 4-hydroxyvalerate (4HV) bound to Rpa3624. A *gray* mesh shows the nonprotein electron density in the active site near the calcium of GVL-soaked crystals, where *green* mesh indicates positive electron density and *red* mesh indicates negative electron density from the difference maps of each modeled ligand. GVL, γ-valerolactone.

(Fig. 7), the predicted tetrahedral reaction intermediate and/or the product.

Models of GVL in either stereochemical configuration (Fig. 7) do not account for the electron density between the substrate and calcium or extending beyond the position of the methyl group. The model for the predicted tetrahedral intermediate (Fig. 6B) better accounts for the electron density near to calcium. In this model, the tetrahedral center is superimposable with the position of phosphate bound to calcium shown in Figure 3B. However, like with GVL, this model does not account for the electron density extending beyond the position of the substrate methyl group.

The electron density can also be modeled with the GVL hydrolysis product, 4-HV (Fig. 6C). In this model, the electron density near the calcium is well-accounted for by the carboxylate group of 4-HV, while the more remote density is adequately represented by placement of the 4-OH and methyl groups. However, since this distal end of 4-HV does not make contacts with the protein backbone, it can likely occupy multiple conformations, accounting for the lower quality of the electron density map in this region. Consequently, the lower real-space correlation coefficient for the product model alone compared to other individual models, particularly the intermediate, supported the need for modeling different ligands into the proposed active site.

Discussion

The motivation for this work was to identify an enzyme from *R. palustris* capable of hydrolyzing the lactone ring of GVL, a solvent that can dissolve plant cell walls into sugars and aromatic molecules for subsequent microbial conversion to fuels and chemicals. Through use of bioinformatics, seven putative enzymes with potential lactonase activity were identified in *R. palustris*, and Rpa3624 emerged as a lactonase with experimentally validated hydrolysis of GVL, other hydrophobic lactones, and some esters. Additional structural and biochemical studies show the unique properties of this lactonase and afford insight into its catalytic mechanism, summarized below.

Rpa3624 is a broad specificity lactonase

Rpa3624 hydrolyzes many lactones with variations in ring size and the nature of the R-group side chain, as well as some esters (Table 1). From comparison of catalytic efficiency values between substrates, Rpa3624 may have evolved to act on more hydrophobic lactones, such as dihydrocoumarin, instead of more water-soluble lactones such as GVL. However, none of the substrates tested had K_M values less than 1 mM, so it is possible that a more tightly binding (preferred) substrate for this enzyme may exist.

The ability of β-propeller lactonases to hydrolyze multiple substrates has been reported previously. The best studied β-propeller lactonase, human PON1, can hydrolyze lactones, esters, and phosphotriesters (23, 24, 34). However, there are several important differences between Rpa3624 and human PON1. First, Rpa3624 has K_M values that are nearly two orders of magnitude higher for γ-butyrolactone and dihydrocoumarin than PON1 (23, 35). This could be due to differences in the
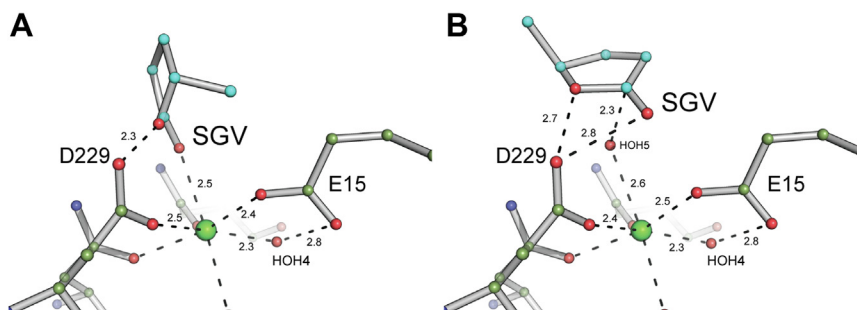

Figure 7. Two plausible orientations of *S*-GVL (SGV) leading to different potential routes to a hydrolysis reaction. Calcium is illustrated as a *green* sphere in the *center* of each frame. Contact distances observed between substrate and other active site entities are indicated. *A*, an orientation where the carbonyl oxygen of SGV coordinates to calcium. *B*, an orientation where a calcium-bound HOH5 is close to the carbonyl carbon of SGV. The SGV lactone is also in equidistant contact with D229, an essential active site residue. GVL, γ-valerolactone.

direction of approach and geometry of the Rpa3624 and PON1 active sites. In PON1, a mobile active site loop of residues Y71 to K81 contributes to binding (34) by almost completely encapsulating the bound ligand (Fig. S6A). In contrast, the 2-HQ–bound structure of Rpa3624 shows that Y211 and R212 from one polypeptide in the dimer extend across the dimer interface and partially define the channel into the active site, which nevertheless remains accessible to solvent (Fig. S6B). Even though the magnitudes of K_M values among comparable substrates are markedly different for Rpa3624 and PON1, both enzymes show lower K_M values for hydrophobic lactones (35). Another distinction is that Rpa3624 does not hydrolyze any tested homoserine lactones, while PON1 does (24, 36).

There are other unrelated lactonases that also possess broad substrate specificity. Lactonases such as AiiA (33), AiiB (37), and GcL (38) from the metallo-β-lactamase–like superfamily also possess broad substrate specificity, but they have an αβ/βα fold and a bimetallic active site that shares no structural similarity with the β-propeller proteins like Rpa3624 and PON1. In addition, the phosphotriesterase-like–lactonases SsoPox (39) and QsdA (40) exhibit broad lactonase specificity but contain an $(\alpha/\beta)_8$ fold and a bimetallic active site. However, these enzymes from other fold families catalyze N-acyl homoserine lactone hydrolysis with catalytic efficiencies in the $10^4 – 10^6$ s^{-1} M^{-1} range, whereas hydrolysis of these substrates by Rpa3624 was not detected under the assay conditions used in this study.

Rpa3624 is not a gluconolactonase

Rpa3624 has been previously annotated as a "gluconolactonase," but this enzyme has no detectable activity on gluconolactone (Table 1). The apparent mis-annotation of proteins related to Rpa3624 could be widespread across bacteria and possibly other organisms, as an analysis of the UniProt database (41) reveals that 3801 of 8418 bacterial reference proteomes (45%) contain a protein predicted to have the same SMP-30/gluconolactonase/luciferin regenerating enzyme (LRE)-like domain as Rpa3624 (42). Results shown in Figure 2 and Table S2 suggest that these domain-sharing enzymes currently annotated as gluconolactonases may include two distinct substrate specificities: those that hydrolyze sugar lactones (true gluconolactonases) and those that are active with hydrophobic substrates. Rpa3624 falls into this latter group of "hydrophobic lactonases," which includes Drp35 (15), PON-X_OCCAL (36), and human PON1 (23, 24). Figure 2 and Table S2 also indicate that primary sequence motifs might be used to better predict whether an annotated

"gluconolactonase" hydrolyzes sugar lactones or hydrophobic lactones. Thus, based on experimental results with hydrophobic substrates and identification of distinctive primary sequence motifs, we propose that the annotation of Rpa3624 and its closest homologs should be modified to "hydrophobic substrate lactonases from the β-propeller fold family."

Ligand binding in Rpa3624 stabilizes a loop near the active site

The three crystal structures of Rpa3624 are overall similar, with backbone RMSD values differing by less than 0.3 Å. Unique among the three structures, the 2-HQ–bound crystal gave defined electron density for residues 77 to 82 and 209 to 212. Both of these loops in the 2-HQ–bound structure partially cover the active site channel, suggesting a "closed" enzyme state in the presence of 2-HQ rather than the "open" state observed in the phosphate- and GVL-bound structures. Specifically, residues 77 to 82 partially cover the active site channel of the same monomer, while residues 209 to 212 partially cover the channel of the other monomer in the homodimer. These loops are not ordered and thus not visible in the GVL-soaked structures, providing a potential explanation for the high K_M for GVL (>500 mM). Within the active sites of the three Rpa3624 structures, only M83, R141, and R267 show different rotamers. These residues may be indirectly involved in forming the "closed" enzyme state.

Structural comparison of Rpa3624 with other β-propeller lactonases

Despite the low amino acid sequence identity between Rpa3624 and other β-propeller lactonases (Table 4), they have high structural similarity in their β-propeller blades. All β-propeller lactonases bind calcium in the active site except for XylC, an enzyme from *Caulobacter crescentus*, which has been shown to bind Fe^{2+} (43, 44). The arrangement of active site residues and waters in XylC leads to octahedral coordination of the Fe^{2+} ion, which is distinct from the pentagonal bipyramidal coordination of the calcium ion in other β-propeller enzymes. LRE is another β-propeller enzyme whose structure has been solved and it binds Mg^{2+} in the predicted active site. However, it is not clear if LRE is a lactonase or possesses a different catalytic activity (45) so it was not included in our comparisons with the other lactonases. Like XylC, the arrangement of active site residues and waters in LRE leads to octahedral coordination of the Mg^{2+} ion.

Table 4
Pairwise sequence identity between β-propeller lactonases with solved structures, created using EMBOSS Needle (64)

Identity	Rpa3624[a]	DFPase[a]	XylC	Drp35[a]	XC5397	SMP-30	PON1[a]
Rpa3624[a]	100						
DFPase[a]	22.2	100					
XylC	21.9	20.1	100				
Drp35[a]	21.5	19.8	17.5	100			
XC5397	21.3	16.8	22.2	18.5	100		
SMP-30	19.5	15.8	30.3	18.7	18.5	100	
PON1[a]	15.7	19.1	14.9	18	14.4	15.6	100

[a] Enzyme has demonstrated activity on hydrophobic, nonsugar lactones.

Some of these enzymes also have a second cation bound close to the active site calcium. For XC5397, PON1, and DFPase, this second calcium is thought to play a structural role (19, 32, 46). The sodium ion in Rpa3624 occupies a similar position as the second calcium in these enzymes and thus may have a similar role. Importantly, the second cation in Rpa3624 is not calcium, based on ICP-MS results from five different preparations that gave an average of 1.00 ± 0.05 equivalents of calcium per polypeptide. The electron density, near-perfect octahedral coordination, and equal average bond length of 2.5 ± 0.2 Å are also consistent with assignment as a sodium ion.

The properties of the Rpa3624 dimer are unique among the β-propeller lactonases. Many of these related enzymes are not reported to oligomerize (15, 21, 47, 48), while XC5397 relies on disulfide bonds and calcium ions to hold its dimer together (19), and PON1 is reported to exist in different oligomerization states which might depend on its association with HDL (49). However, the Rpa3624 dimer forms a different interface than XC5397 and appears to utilize a domain swapping-like mechanism to form a "closed" enzyme state (Fig. S6). These characteristics could be useful for informing targeted efforts to improve substrate binding by Rpa3624.

The positions of most calcium-binding residues for Rpa3624, Drp35, PON1, DFPase, and XC5397 align well (Fig. 8). Thus, the electrostatic environment of the active site is likely similar between these enzymes. For example, the phosphate bound in PON1 (PDB 3SRE, (34)) and in Rpa3624 are found in nearly identical positions in the aligned structures. Furthermore, waters in the active sites of Drp35 (PDB 2DG1, (15)), DFPase (PDB 3O4P, (47)), and XC5397 (PDB 3DR2, (19)) occupy the same positions as two of the phosphate oxygens in Rpa3624. Since the phosphate in PON1 has been proposed to represent the position of a tetrahedral intermediate in the active site (34) and the phosphate in Rpa3624 is

Figure 8. Overlay of related β-propeller lactonase active sites. Rpa3624 (PDB 7RIS) shown in *green* transparent, outlined ball-and-stick with calcium shown as a *green sphere*, and coordinated water molecules shown as *red spheres*. Positions of E15, coordinated water HOH4, and D229 in the Rpa3624 active site are indicated. Other enzymes are shown as lines: *green*, (PON1, PDB 3SRE); *cyan* (Drp35, PDB 2DG1); *magenta* (XC5397, 3DR2); *gold* (DFPase, PDB 3O4P).

displaced by either 2-HQ or GVL according to ^{31}P-NMR and crystallography data, we used the positions of phosphate atoms to build models for various arrangements of substrate, a putative tetrahedral intermediate, and product bound in the Rpa3624 active site.

Proposed Rpa3624 reaction mechanism

Multiple mechanisms have been proposed for the β-propeller lactonases (15, 32, 34, 50, 51), and no consensus has arisen thus far. These differ in the placement of the substrate carbonyl bond, the activated water nucleophile used to attack the carbonyl carbon of the lactone (or ester) bond, as well as the identity of the amino acid(s) responsible for activating the water nucleophile. While each of these mechanisms are plausible, the data on Rpa3624 permits consideration of an additional possibility.

For Rpa3624, there are two positions for the substrate and activated water nucleophile compatible with the electron density. In one placement (Fig. 7A), the carbonyl oxygen of the GVL lactone is coordinated to calcium in a position and orientation like that in both Rpa3624 and PON1 (34) complexed to the inhibitor 2-HQ (Fig. 3C). However, the nearest water in all Rpa3624 structures, HOH4, is located on the opposite side of the active site and too far (>5 Å) from the carbonyl carbon of the substrate to be directly involved in nucleophilic attack. Modeling to include a water in a potential nucleophile site between E15 and D229 of Rpa3624 did not provide a satisfactory match to the electron density. Because this placement of substrate matches the orientation of the inhibitor 2-HQ, and because there is a lack of evidence for productive water nucleophile placement, we propose that this orientation of substrate might not lead to catalysis in Rpa3624.

In a second placement of substrate and water nucleophile (Fig. 7B), the Rpa3624 electron density supported modeling a water (HOH5) bound to calcium with GVL residing above this water, such that GVL no longer makes direct contact with the calcium. Here, the unbound carboxylate O from D229 would be equidistant between the carbonyl O and lactone ring O of the substrate (~2.7 Å). Moreover, HOH5 is modeled to lie ~2.3 Å from the carbonyl C of the substrate. This close placement of reacting atoms could allow water deprotonation, nucleophilic attack of the substrate, and protonation-assisted cleavage of the lactone ring to proceed in a near simultaneous manner.

For Rpa3624 and Drp35 (15), the pH dependence of activity (Fig. 5) suggests an acidic residue (*i.e.*, E15 or D229 in Rpa3624) is involved in water nucleophile activation. Mutational analysis further shows that Rpa3624 catalysis does not tolerate a D to E substitution at residue D229 (Table 3), even though this D229E variant retains some calcium-binding ability, supporting the need for close positioning of D229 in the active site. In contrast, an Rpa3624 E15D variant retains lactonase activity, suggesting accurate positioning of the acid group of E15 is not as important for activity.

Figure 9 presents a proposed reaction mechanism for Rpa3624, which involves placement of the activated water
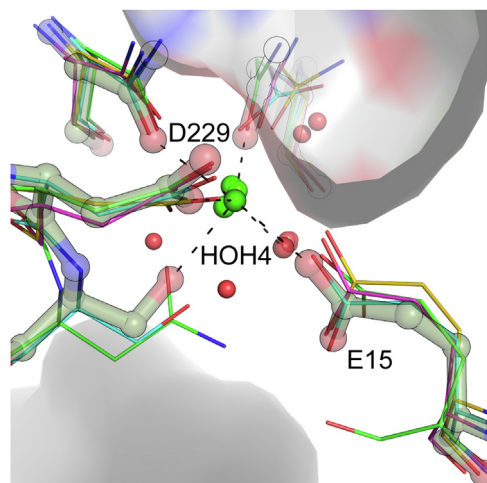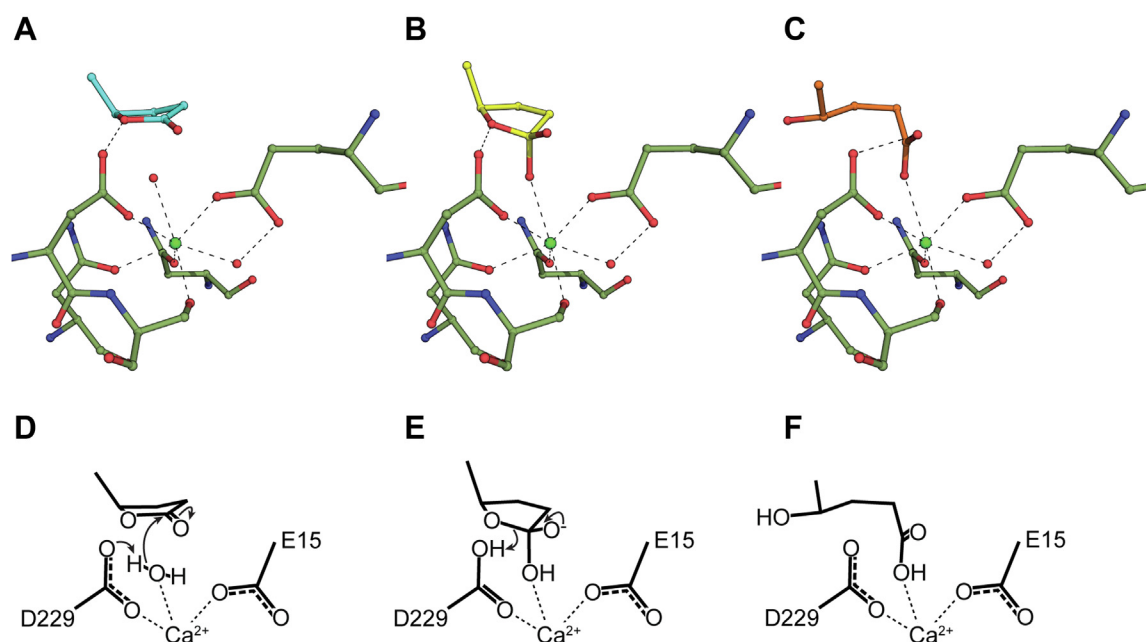
Figure 9. One possible mechanism for the Rpa3624 reaction based on the initial binding orientation for substrate shown in Figure 7B. Models of reaction steps are shown in panels (*A–C*) (PDB 8DK0, 8DJF, and 8DJZ), with corresponding movement of protons and electrons shown in panels (*D–F*). *A* and *D*, D229 deprotonates the calcium-bound water molecule, activating the water for nucleophilic attack of the carbonyl carbon of the ester bond. *B* and *E*, After tetrahedral intermediate formation, the lactone ring undergoes protonation-assisted cleavage by D229 to complete the catalytic cycle (*C* and *F*).

nucleophile bound to calcium, an orientation of substrate above this water, and the identity of the amino acid responsible for activating the water nucleophile. This mechanism differs from earlier proposals for other lactonases in several important aspects. First, our proposal suggests that the water nucleophile is bound directly to the calcium ion, but not simultaneously with substrate as proposed for Drp35 (15) and in some variations of the PON1 mechanism (50). Second, the initial placement of substrate in the Rpa3624 mechanism involves the substrate carbonyl bond interacting with active site residues instead of the calcium ion. Finally, Rpa3624 is proposed to use different amino acids for water nucleophile activation than other enzymes. Rpa3624 has D229 in position to interact with both the calcium-bound water nucleophile and the substrate lactone ring O atom. Moreover, Rpa3624 has an asparagine in place of catalytic base D138 proposed for Drp35 (15) and lacks the active site histidine residues seen in PON1 (32). Interestingly, prior mutational analyses suggest that the Rpa3624 D229 counterpart may play a role in water deprotonation in both Drp35 (15, 50) and PON1 (50, 52). In addition, the identity and steric arrangement of Rpa3624 E15 and D229 counterparts is conserved across all β-propeller lactonases included in Table 4, suggesting that one or both of these residues has a likely role in catalysis in all of these enzymes.

Conclusion

This work establishes that Rpa3624 is a broad specificity lactonase that hydrolyzes GVL. Rpa3624 also shows preference for many other hydrophobic substrates albeit with high K_M values, possibly due to an open, nonselective channel to the active site. In addition, Rpa3624 does not catalyze the hydrolysis of gluconolactone or *N*-acyl homoserine lactones seen in related enzymes. Analysis of mutational results and crystal structures support Rpa3624 residue D229 as an exquisitely positioned catalytic residue. These properties impart a utility for Rpa3624 in the treatment of biomass-derived fermentation substrates contaminated with GVL, while leaving open the question of what other metabolic impacts this broad specificity lactonase might have during microbial growth.

Experimental procedures

Strains and media

R. palustris strain CGA009 (53) was grown in PM medium (54) with 10.5 mM GVL (0.1% v/v) as the sole organic carbon source and 10 mM NaHCO₃ supplemented as an electron sink (55). Medium was prepared fresh before growth experiments, as our mass spectrometry showed that GVL spontaneously converts to 4-HV on relatively short time scales (Fig. 1), contrary to a previous report (11). Cultures were grown at 30 °C, either photoheterotrophically in filled and sealed Hungate culture tubes with stir bars in front of incandescent tungsten lamps outputting approximately 10 W/m² or aerobically in shake flasks. Cell density was monitored using a Klett-Summerson photoelectric colorimeter. Routine cloning was performed using NEBuilder HiFi DNA Assembly Master Mix and NEB5α *E. coli* cells grown in LB medium containing 50 μg/ml of kanamycin at 37 °C.

Preparation of R. palustris *whole cell extract*

Whole cell extract was produced from *R. palustris* CGA009 grown aerobically in PM-GVL medium described above. Pelleted cells from 250 ml culture were resuspended in 5 ml of 20 mM Hepes (4-(2-hydroxyethyl)-1-piperazineethanesulfonic acid), pH 7.5, containing 300 mM NaCl, 1 mM TCEP (tris(2-

carboxyethyl)phosphine), and 1% glycerol. The cell suspension was sonicated using a Branson Sonifier 450 for 25 cycles with 30 on and 30 off using a 50% duty cycle on the maximum power setting for the microtip attachment. Cell debris was removed by centrifugation at 20,000*g* for 30 min at 4 °C. Protein concentration of the cell extract was determined using the Bio-Rad Protein Assay with bovine serum albumin (BSA) as a standard.

HPLC–tandem mass spectrometry

Analysis of the hydrolysis of GVL to 4-HV by *R. palustris* whole cell extract was performed using a Shimadzu triple quadrupole LC-MS (Nexera XR HPLC-8045 MS/MS). Three technical replicates were prepared that contained 1 mM GVL and 1 mg/ml *R palustris* whole cell extract in 20 mM Hepes, pH 7.5, containing 300 mM NaCl, 1 mM TCEP, and 1% (v/v) glycerol. Injections of 0.5 μl were separated using a Kinetex 2.6 μm C18 100 Å 50 × 2.1 mm column at 0.5 ml/min. The mobile phase started at 99% of 0.25% formic acid and 1% of methanol, ramped up to 5% methanol at 1 min, 20% methanol at 1.5 min, 95% methanol at 2.5 min, then returned to 1% methanol between 2.8 and 3.2 min. The total method time was 5 min. 4-HV eluted at 0.88 min and GVL eluted at 1.21 min. 4-HV was identified by measuring ions in the positive mode that had a parent *m/z* of 119.3 and a product *m/z* of 83.1. GVL was identified by measuring ions in the positive mode that had a parent *m/z* of 101.1 and a product *m/z* of 60.1. Control replicates contained 1 mM GVL in the same buffer as above without cell extract. Quantification was performed in the Lab Solutions software by calculating the total area under the curve for product ion counts around the retention time of each compound. Standard curves for GVL and 4-HV were used to calculate concentrations in samples and controls. 4-HV was prepared by increasing the pH of 2 M GVL to pH 12 with concentrated NaOH and incubation for 1 h at room temperature (56). After hydrolysis, the 4-HV solution was adjusted to pH 8 with concentrated HCl.

Expression of candidate lactonases

Each of the seven candidate lactonase genes (*rpa0798*, *rpa1095*, *rpa2488*, *rpa2779*, *rpa4424*, *rpa4673*, and *rpa3624*) was cloned into pVP302K (57), which adds an N-terminal His$_8$ tag to the protein coding sequence, and expressed in *E. coli* B834–harboring pRARE (58). Cells were grown in autoinduction medium ZMS-80155 (59) supplemented with 50 μg/ml kanamycin and 20 μg/ml chloramphenicol. The ZMS-80155 medium contains 1% N-Z Amine AS, 50 mM phosphate, 20 mM succinate, 0.8% glycerol, 0.015% glucose, 0.5% α-lactose, 2 mM MgSO$_4$, a trace metals mix (59), and a vitamin mix (60). Cultures were grown at 30 °C to A$_{600}$ ~7, at which point they were chilled on ice. Cells were pelleted by centrifugation at 6000*g* for 10 min at 4 °C. The cell pellets were then resuspended in 20 mM Hepes, pH 7.5, containing 300 mM NaCl, 1 mM TCEP, and 1% glycerol. Cell suspensions were sonicated using a Branson Sonifier 450 for 30 min at 25% duty cycle on the max power setting for the microtip

attachment. Cell debris was separated from the cell lysate by centrifugation at 20,000*g* for 30 min at 4 °C.

Expression and purification of Rpa3624

Rpa3624 was expressed as described above, except the autoinduction medium and Hepes storage buffer contained an additional 1 mM CaCl$_2$. The cell lysate, prepared as described above, was passed through a Bio-Rad Econo-Pac gravity-flow chromatography column filled with 10 ml of Qiagen Ni-NTA agarose beads pre-equilibrated with Hepes storage buffer. The column was washed with 20 mM Hepes, pH 7.5, containing 200 mM NaCl, 25 mM imidazole, 1 mM CaCl$_2$, and 0.5 mM TCEP. Rpa3624 was eluted in the same buffer modified to contain 300 mM NaCl and 500 mM imidazole. All column chromatography was carried out at 4 °C. Elution fractions containing protein as determined by Ponceau staining were combined for overnight dialysis at 4 °C in 20 mM Hepes, pH 7.5, containing 300 mM NaCl, 1 mM CaCl$_2$, 1 mM TCEP, and 1% (v/v) glycerol. Approximately, 0.025 mg/ml TEV protease was added to each dialysis sample to remove the His$_8$ tag from Rpa3624. After dialysis, the TEV protease reaction was allowed to continue for approximately 24 h at room temperature. The sample was then run through an additional round of nickel affinity chromatography to remove the cleaved His$_8$ tag and the His-tagged TEV protease. The flow-through containing Rpa3624 was collected and concentrated using an Amicon Ultra-15 centrifugal filter unit to ~1 mg/ml for kinetic analysis and to ~15 mg/ml for ICP-MS and crystallography. Protein concentration was determined using the Bio-Rad Protein Assay. The standard was an Rpa3624 sample whose concentration was determined by ICP-MS measurement of sulfur content, which derives from cysteine and methionine residues. Protein purity was assessed by SDS-PAGE.

Enzyme kinetics

Assays of lactone and ester substrates (γ-butyrolactone, γ-valerolactone, γ-decanolactone, δ-valerolactone, δ-nonalactone, mevalonolactone, ε-caprolactone, *p*-coumaryl homoserine lactone, 3-oxo-hexanoyl homoserine lactone, phenyl acetate, ethyl acetate, octyl acetate) were performed using a colorimetric assay (35). Hydrolysis results in carboxylic acid formation, and at near-neutral pH, this leads to proton release which can be monitored by a pH indicator. A typical assay included 185 μl of 2.5 mM bicine, pH 8.3, containing 150 mM NaCl, 1 mM CaCl$_2$, 200 μM *m*-cresol purple from a 60 mM stock in DMSO, and additional DMSO to total 0.5% (v/v); a 10 μl aliquot of the lactone or ester dissolved in DMSO at various concentrations; and 5 μl of purified enzyme diluted into dialysis buffer supplemented with 0.1 mg/ml BSA. Lactone and ester substrates were dissolved in DMSO to prevent spontaneous hydrolysis during storage. BSA was added to the enzyme dilutions because in the absence of BSA, activity of the diluted enzyme sample decreased over time, presumably due to adsorption to the storage tube (61). Standard curves for hydrolysis reactions were generated by mixing 185 μl of the assay buffer, 10 μl acetic acid in DMSO at various

concentrations, and 5 µl of the dialysis buffer with BSA but without enzyme. Cresol purple absorbance at 577 nm was measured over time, and lactone plus enzyme samples were corrected for the rate of spontaneous hydrolysis as measured in lactone blank samples. Lactone hydrolysis measurements were recalibrated to the standard curve at each time point because of natural acidification of all samples over time presumably due to equilibration with CO_2 in air (35). For some substrates at high concentrations, more buffering capacity was added to the lactonase buffer to ensure spontaneous hydrolysis did not surpass the dynamic range of the assay.

Dihydrocoumarin hydrolysis followed an increase in absorbance at 270 nm, where the difference in molar absorptivity between dihydrocoumarin and the product is 1295 M^{-1} cm^{-1} (62). A typical assay consists of 190 µl of 50 mM Tris, pH 8, containing 150 mM NaCl and 1 mM $CaCl_2$, 5 µl dihydrocoumarin in DMSO at various concentrations, and 5 µl of purified enzyme diluted into dialysis buffer with 0.1 mg/ml BSA. Measurements were corrected for the spontaneous hydrolysis of dihydrocoumarin in blank samples that replaced the 5 µl enzyme with 5 µl dialysis buffer with BSA. Assays at different pH values used the same conditions, but replaced 50 mM Tris, pH 8 with 50 mM of different buffers: acetic acid (pH 4.5, 5, 5.5); MES (pH 5.75, 6); Pipes (pH 6.5); Mops (pH 7); Hepes (pH 7.5); bicine (pH 8.5); and Ches (pH 9).

All kinetic experiments were performed in technical triplicates, in which absorbance was measured every 15 s for 5 min using a Tecan Infinite M1000 plate reader. Rates were only calculated from initial linear hydrolysis rates if the rates slowed over the 5 min. Measurements at 577 nm used Thermo Scientific Nunc Microwell 96-well clear flat-bottom plates. Dihydrocoumarin assays at 270 nm used Greiner UV-Star 96-well clear flat-bottom plates, which have a measured path length of 6.2 mm.

Kinetic parameters were determined by fitting data to the Michaelis-Menten equation using GraphPad PRISM 8. Substrates were assayed at four concentrations, approximating 0.5 K_M, K_M, 2 K_M, and 3 K_M, using three biological replicates of purified Rpa3624, and the parameters for the best fit are reported with the 95% confidence interval. In some cases, each replicate was fit to the Michaelis-Menten equation and the mean ± SD for the kinetic parameters is reported. For some substrates and at some pH values, the data were better fit with a linear model than the Michaelis-Menten equation (Extra sum of squares F test, $p > 0.05$), so estimates of k_{cat}/K_M only were determined from a linear fit of the data points.

Phylogenetic tree construction

A list of Rpa3624-related sequences was assembled by PaperBLAST (63) and a literature search for gluconolactonases with evidence of lactonase activity (Table S2). Clustal Omega (64) and RAxML-NG (65) were used to create a maximum-likelihood phylogenetic tree of these sequences with 1000 bootstraps and AiiA specified as the outgroup using the CIPRES Science Gateway (66).

Crystallization, X-ray diffraction, and refinement

Crystallization experiments and structure determination were conducted in the Collaborative Crystallography Core in the Department of Biochemistry at the University of Wisconsin. All crystallization screens and optimizations were conducted at 293K in MRC SD-2 crystallization plates set with a STP Labtech Mosquito crystallization robot. Hampton IndexHT and Molecular Dimensions JCSG+ were used as general screens. Crystals were individually harvested in MiTeGen MicroMounts and cryopreserved by direct immersion in liquid nitrogen. Diffraction screening and data collection occurred at LS-CAT and GMCA@APS beamlines at the Advanced Photon Source, Argonne National Labs. Data from 21ID-D was collected on a Dectris Eiger X9 and data from 21ID-F was collected on a Rayonix MX3000HE. Diffraction data was reduced and scaled using XDS (67) and XSCALE (68). Most computational manipulations were performed in the Phenix suite of crystallography programs (69). Models were improved using alternating rounds of phenix.refine (70) and rebuilding in Coot (71). The structures were validated with MOLPROBITY. All crystals leading to the reported structures belonged to space group P3$_2$21, with a and b axes around 45 Å and c around 195 Å. PISA interface analysis (29, 30) of these trigonal crystals consistently reveals an extensive crystal packing interface of around one thousand $Å^2$. Another crystal form with a dimer in the asymmetric unit sometimes grew in crystallization solutions containing tartarate.

The crystallographic phase problem was solved from single-wavelength anomalous diffraction (SAD) at 1.5349 Å using data from a Ho-derivatized crystal. The sample was prepared by adding 5 mM holmium (III) chloride to a 10 mg/ml solution of Rpa3624 in 50 mM sodium Hepes buffer, 50 mM NaCl, 0.3 mM TCEP and incubating it overnight at 277K. The sample was dialyzed against 0.1 mM holmium chloride, 5 mM Hepes buffer, 50 mM NaCl, 0.3 mM TCEP and brought to 10 mg/ml with a centrifugal concentrator. Crystals were grown from 18% PEG 3350, 0.1 M bis-tris methane (2-[Bis(2-hydroxyethyl)amino]-2-(hydroxymethyl)propane-1,3-diol) buffer at pH 6.5. Diffraction data was on 2019-11-2 at APS beamline 21ID-D. A single strong holmium site was located by phenix.hyss (72). The holmium ion site was later confirmed to arise from the anticipated replacement of the active-site calcium ion. The experimental map (figure of merit 0.443) was partially traced using phenix.autosolve (73). The trace was extended with arp/warp (74). Combining phase information from the partial model and the holmium derivative using Phenix MD-SAD improved the map further (FOM 0.732).

Native data for refinement and deposition (7RIS) came from a crystal grown by combining 200 nl of protein at 10.5 mg/ml, 250 nl reservoir composed of 20% PEG 3350, 0.1 M bis-tris methane buffer at pH 6.5. The crystal was cryopreserved in reservoir solution supplemented to 30% PEG 3350. Data was collected at APS beamline 21ID-D on 2019-11-02. The structure could be solved using the MR-SAD model by either molecular replacement or rigid body refinement.

The best inhibitor-bound data set (7RIZ) was grown by incubating 9.2 mg/ml protein with 5 mM 2-HQ for an hour prior to crystallization setup, where 200 nl of protein was mixed with 100 nl reservoir solution containing 24% PEG 3350, 0.2 M CaCl2, 0.1 M bis-tris methane buffer at pH 6.5. The crystal was cryopreserved with reservoir solution supplemented to 30% PEG 3350 and 5 mM 2-HQ. Data was collected at APS beamline 21ID-D on 2020-07-25.

Substrate-soak data sets were collected at APS beamline 21ID-F on 2021-11-10, on crystals grown from 20% PEG 3350, 0.2 M NaCl, 0.1 M sodium acetate buffer, pH 4.5 or 20% PEG 3350, 0.2 M CaCl2, 0.1 M bis-tris methane buffer, pH 6.5. Crystals soaked in both *R*- and *S*-GVL were screened for diffraction power. The best diffraction was obtained from a crystal soaked for 360 s in reservoir solution supplemented with 20% *S*-GVL. No additional cryoprotection was necessary.

Models of the two possible transition state stereoisomers were sketched in ChemDraw, exported in SDF format, and optimized in phenix.elbow (75). All ligand models were further refined using the GRADE server (76), which uses the Cambridge Crystallographic Data Center program MOGUL (77). Many different poses of possible substrates, transition states, and products were built into the largest difference electron density, proximal to the active site calcium. A combination of interactive building and automatic docking in phenix.ligandfit (78) provided a small number of candidates that reasonably fit the electron density and made chemical sense. Three of those candidates were refined to completion and are reported in Table 1.

Size-exclusion chromatography

Size-exclusion chromatography was used to determine the oligomerization state of native Rpa3624. A Phenomenex bio-Zen size-exclusion column (SEC-2 1.8 μm 150 Å 150 × 4.6 mm) hooked up to a Shimadzu Nexera XR HPLC system set to 0.7 μl injections and a 0.3 ml/min flow rate was used for sample separation. The mobile phase was 20 mM Hepes, pH 7.5, containing 300 mM NaCl, 1 mM TCEP, and 1% (v/v) glycerol. Protein retention times were determined by absorbance at 280 nm as measured by a Shimadzu SPD-M20A photodiode array detector. A standard curve was created by plotting $\log_{10}$ MW *versus* retention time for seven protein standards. Standards were purchased from Sigma-Aldrich (bovine heart cytochrome *c*, *Glycine max* trypsin inhibitor, bovine erythrocyte carbonic anhydrase, and BSA) or GE Healthcare (RNase A, ovalbumin, and conalbumin; contained in a gel filtration calibration kit). The MW of three biological replicates of Rpa3624 was determined from the linear fit of this standard curve.

Inductively coupled plasma mass spectrometry

Concentrated samples of purified Rpa3624 (∼10 mg/ml) were dialyzed overnight in 30 mM Tris, pH 8, containing 100 mM NaCl. Samples were sent to the Wisconsin State Laboratory of Hygiene in acid-cleaned microfuge tubes for trace metal analysis using ICP-MS. Protein concentration was determined from sulfur concentration by ICP-MS, as sulfur corresponds to the cysteine and methionine residues in Rpa3624. ICP-MS results are presented as mol of element per mol of protein monomer.

^{31}P-NMR

Purified Rpa3624 (∼13 mg/ml protein) was analyzed at the Nuclear Magnetic Resonance Facility at Madison. ^{31}P-NMR spectra were collected using a Bruker Avance III HD, 600 MHz machine, and 5 mm cryoprobes. Data was collected for approximately 24 h for each sample (65,000 scans, DE 30 μs). The inhibitor 2-HQ was added from a 540 mM stock in DMSO for a final concentration of 9 mM.

Site-directed mutagenesis

All mutations were constructed using a version of *rpa3624* that had been codon optimized for *E. coli* (Integrated DNA Technologies). Mutations were introduced by creating primers with the necessary codon changes near their 5′ ends, which were used to create overlapping PCR fragments of *rpa3624* with the desired mutation. These fragments were combined with pVP302K using NEBuilder HiFi DNA Assembly and were transformed into *E. coli* NEB5α competent cells to prepare plasmid. Mutations were verified by sequencing.

Inhibition by 2-HQ

Inhibition of dihydrocoumarin hydrolysis by 2-HQ was studied using the *m*-cresol purple assay in the presence of 0, 2, 4, and 8 mM 2-HQ, added directly to the lactonase assay buffer at a 1:100 dilution from a stock in DMSO.

Data availability

The atomic coordinates and structure factors (codes 7RIS, 7RIZ, 8DK0, 8DJF, 8DJZ) have been deposited in the Protein Data Bank (http://wwpdb.org/). Frame data has been deposited in (https://www.proteindiffraction.org).

Abbreviations—The abbreviations used are: 2-HQ, 2-hydroxyquinoline; 4-HV, 4-hydroxyvalerate; BSA, bovine serum albumin; GVL, γ-valerolactone; ICP-MS, inductively coupled plasma mass spectrometry; LRE, luciferin regenerating enzyme; MW, molecular weight; SAD, single-wavelength anomalous diffraction; TCEP, tris(2-carboxyethyl)phosphine.

References

1. Bublitz, C., and Lehninger, A. L. (1961) The role of aldonolactonase in the conversion of L-gulonate to L-ascorbate. *Biochim. Biophys. Acta* **47**, 288–297
2. Okamura-Abe, Y., Abe, T., Nishimura, K., Kawata, Y., Sato-Izawa, K., Otsuka, Y., *et al.* (2016) Beta-ketoadipic acid and muconolactone production from a lignin-related aromatic compound through the protocatechuate 3,4-metabolic pathway. *J. Biosci. Bioeng.* **121**, 652–658
3. Watanabe, S., Saimura, M., and Makino, K. (2008) Eukaryotic and bacterial gene clusters related to an alternative pathway of nonphosphorylated L-rhamnose metabolism. *J. Biol. Chem.* **283**, 20372–20382
4. Reichert, S., Ebner, P., Bonetti, E. J., Luqman, A., Nega, M., Schrenzel, J., *et al.* (2018) Genetic adaptation of a mevalonate pathway deficient mutant in Staphylococcus aureus. *Front. Microbiol.* **9**, 1539
5. Cook, C., Whichard, L. P., Wall, M., Egley, G. H., Coggon, P., Luhan, P. A., *et al.* (1972) Germination stimulants. II. Structure of strigol, a potent seed germination stimulant for witchweed (Striga lutea). *J. Am. Chem. Soc.* **94**, 6198–6199
6. Eberhard, A., Burlingame, A. L., Eberhard, C., Kenyon, G. L., Nealson, K. H., and Oppenheimer, N. (1981) Structural identification of autoinducer of Photobacterium fischeri luciferase. *Biochemistry* **20**, 2444–2449
7. Horinouchi, S., and Beppu, T. (1994) A-factor as a microbial hormone that controls cellular differentiation and secondary metabolism in Streptomyces griseus. *Mol. Microbiol.* **12**, 859–864
8. Sheehan, J. C., and Ledis, S. L. (1973) Total synthesis of a monocyclic peptide lactone antibiotic, etamycin. *J. Am. Chem. Soc.* **95**, 875–879
9. Wencewicz, T. (2018) Beta-lactam and beta-lactone antibiotics from plant microbiomes. *FASEB J.* **32**, 257.1
10. Luterbacher, J. S., Rand, J. M., Alonso, D. M., Han, J., Youngquist, J. T., Maravelias, C. T., *et al.* (2014) Nonenzymatic sugar production from biomass using biomass-derived γ-valerolactone. *Science* **343**, 277
11. Horváth, I. T., Mehdi, H., Fábos, V., Boda, L., and Mika, L. T. (2008) γ-Valerolactone—a sustainable liquid for energy and carbon-based chemicals. *Green Chem.* **10**, 238–242
12. Bottoms, S., Dickinson, Q., McGee, M., Hinchman, L., Higbee, A., Hebert, A., *et al.* (2018) Chemical genomic guided engineering of gamma-valerolactone tolerant yeast. *Microb. Cell Fact.* **17**, 5
13. Dong, Y. H., Xu, J. L., Li, X. Z., and Zhang, L. H. (2000) AiiA, an enzyme that inactivates the acylhomoserine lactone quorum-sensing signal and attenuates the virulence of Erwinia carotovora. *Proc. Natl. Acad. Sci. U. S. A.* **97**, 3526–3531
14. Fetzner, S. (2015) Quorum quenching enzymes. *J. Biotechnol.* **201**, 2–14
15. Tanaka, Y., Morikawa, K., Ohki, Y., Yao, M., Tsumoto, K., Watanabe, N., *et al.* (2007) Structural and mutational analyses of Drp35 from Staphylococcus aureus: a possible mechanism for its lactonase activity. *J. Biol. Chem.* **282**, 5770–5780
16. Kataoka, M., Honda, K., and Shimizu, S. (2000) 3,4-Dihydrocoumarin hydrolase with haloperoxidase activity from Acinetobacter calcoaceticus F46. *Eur. J. Biochem.* **267**, 3–10
17. Kanagasundaram, V., and Scopes, R. (1992) Isolation and characterization of the gene encoding gluconolactonase from Zymomonas mobilis. *Biochim. Biophys. Acta* **1171**, 198–200
18. Reshma, S. V., Sathyanarayanan, N., and Nagendra, H. G. (2017) Characterization of a hypothetical protein YVRE from Bacillus subtilis indicates its key role as glucono-lactonase in pentose phosphate pathway and glucose metabolism. *Bioinformation* **13**, 430–438
19. Chen, C. N., Chin, K. H., Wang, A. H., and Chou, S. H. (2008) The first crystal structure of gluconolactonase important in the glucose secondary metabolic pathways. *J. Mol. Biol.* **384**, 604–614
20. Sutter, J.-M., Johnsen, U., and Schönheit, P. (2017) Characterization of a pentonolactonase involved in D-xylose and L-arabinose catabolism in the haloarchaeon Haloferax volcanii. *FEMS Microbiol. Lett.* **364**
21. Boer, H., Andberg, M., Pylkkänen, R., Maaheimo, H., and Koivula, A. (2019) *In vitro* reconstitution and characterisation of the oxidative D-xylose pathway for production of organic acids and alcohols. *AMB Express* **9**, 48
22. Onakunle, O. A., Knowles, C. J., and Bunch, A. W. (1997) The formation and substrate specificity of bacterial lactonases capable of enantioselective resolution of racemic lactones. *Enzyme Microb. Technology* **21**, 245–251
23. Billecke, S., Draganov, D., Counsell, R., Stetson, P., Watson, C., Hsu, C., *et al.* (2000) Human serum paraoxonase (pon1) isozymes Q and R hydrolyze lactones and cyclic carbonate esters. *Drug Metab. Dispos.* **28**, 1335
24. Draganov, D. I., Teiber, J. F., Speelman, A., Osawa, Y., Sunahara, R., and La Du, B. N. (2005) Human paraoxonases (PON1, PON2, and PON3) are lactonases with overlapping and distinct substrate specificities. *J. Lipid Res.* **46**, 1239–1247
25. Oshlag, J. Z. (2018) *Tiny Purple Toxin Eater: Exploring and Expanding the Metabolic Capacity of Rhodopseudomonas palustris.* Doctor of Philosophy, University of Wisconsin-Madison
26. Wang, L. H., Weng, L. X., Dong, Y. H., and Zhang, L. H. (2004) Specificity and enzyme kinetics of the quorum-quenching N-Acyl homoserine lactone lactonase (AHL-lactonase). *J. Biol. Chem.* **279**, 13645–13651
27. Fishbein, W. N., and Bessman, S. P. (1966) Purification and properties of an enzyme in human blood and rat liver Microsomes catalyzing the formation and hydrolysis of γ-lactones: II. Metal ion effects, kinetics, and equilibria. *J. Biol. Chem.* **241**, 4842–4847
28. Belinskaya, T., Pattabiraman, N., diTargiani, R., Choi, M., and Saxena, A. (2012) Differences in amino acid residues in the binding pockets dictate substrate specificities of mouse senescence marker protein-30, human paraoxonase1, and squid diisopropylfluorophosphatase. *Biochim. Biophys. Acta* **1824**, 701–710

ASBMB

29. Krissinel, E., and Henrick, K. (2007) Inference of macromolecular assemblies from crystalline state. *J. Mol. Biol.* **372**, 774–797

30. Elias, M., and Tawfik, D. S. (2012) Divergence and convergence in enzyme evolution: parallel evolution of paraoxonases from quorum-quenching lactonases. *J. Biol. Chem.* **287**, 11–20

31. Raaflaub, J. (1956) Applications of metal buffers and metal indicators in biochemistry. *Methods Biochem. Anal.* **3**, 301–325

32. Harel, M., Aharoni, A., Gaidukov, L., Brumshtein, B., Khersonsky, O., Meged, R., *et al.* (2004) Structure and evolution of the serum paraoxonase family of detoxifying and anti-atherosclerotic enzymes. *Nat. Struct. Mol. Biol.* **11**, 412–419

33. Momb, J., Wang, C., Liu, D., Thomas, P. W., Petsko, G. A., Guo, H., *et al.* (2008) Mechanism of the quorum-quenching lactonase (AiiA) from Bacillus thuringiensis. 2. Substrate modeling and active site mutations. *Biochemistry* **47**, 7715–7725

34. Ben-David, M., Elias, M., Filippi, J. J., Dunach, E., Silman, I., Sussman, J. L., *et al.* (2012) Catalytic versatility and backups in enzyme active sites: the case of serum paraoxonase 1. *J. Mol. Biol.* **418**, 181–196

35. Khersonsky, O., and Tawfik, D. S. (2005) Structure–reactivity studies of serum paraoxonase PON1 suggest that its native activity is lactonase. *Biochemistry* **44**, 6371–6382

36. Bar-Rogovsky, H., Hugenmatter, A., and Tawfik, D. S. (2013) The evolutionary origins of detoxifying enzymes: the mammalian serum paraoxonases (PONs) relate to bacterial homoserine lactonases. *J. Biol. Chem.* **288**, 23914–23927

37. Liu, D., Thomas, P. W., Momb, J., Hoang, Q. Q., Petsko, G. A., Ringe, D., *et al.* (2007) Structure and specificity of a quorum-quenching lactonase (AiiB) from Agrobacterium tumefaciens. *Biochemistry* **46**, 11789–11799

38. Bergonzi, C., Schwab, M., Naik, T., and Elias, M. (2019) The structural determinants accounting for the broad substrate specificity of the quorum quenching lactonase GcL. *Chembiochem* **20**, 1848–1855

39. Hiblot, J., Gotthard, G., Elias, M., and Chabriere, E. (2013) Differential active site loop conformations mediate promiscuous activities in the lactonase SsoPox. *PLoS One* **8**, e75272

40. Afriat, L., Roodveldt, C., Manco, G., and Tawfik, D. S. (2006) The latent promiscuity of newly identified microbial lactonases is linked to a recently diverged phosphotriesterase. *Biochemistry* **45**, 13677–13686

41. Bursteinas, B., Britto, R., Bely, B., Auchincloss, A., Rivoire, C., Redaschi, N., *et al.* (2016) Minimizing proteome redundancy in the UniProt Knowledgebase. *Database (Oxford)* **2016**, baw139

42. Mistry, J., Chuguransky, S., Williams, L., Qureshi, M., Salazar, G. A., Sonnhammer, E. L. L., *et al.* (2021) Pfam: the protein families database in 2021. *Nucleic Acids Res.* **49**, D412–D419

43. Paakkonen, J., Penttinen, L., Andberg, M., Koivula, A., Hakulinen, N., Rouvinen, J., *et al.* (2021) Xylonolactonase from Caulobacter crescentus is a mononuclear nonheme iron hydrolase. *Biochemistry* **60**, 3046–3049

44. Paakkonen, J., Hakulinen, N., Andberg, M., Koivula, A., and Rouvinen, J. (2022) Three-dimensional structure of xylonolactonase from Caulobacter crescentus: a mononuclear iron enzyme of the 6-bladed beta-propeller hydrolase family. *Protein Sci.* **31**, 371–383

45. Hosseinkhani, S., Emamgholi Zadeh, E., Sahebazzamani, F., Ataei, F., and Hemmati, R. (2017) Luciferin-regenerating enzyme crystal structure is solved but its function is still unclear. *Photochem. Photobiol.* **93**, 429–435

46. Hartleib, J., Geschwindner, S., Scharff, E. I., and RÜTerjans, H. (2001) Role of calcium ions in the structure and function of the di-isopropylfluorophosphatase from Loligo vulgaris. *Biochem. J.* **353**, 579–589

47. Elias, M., Liebschner, D., Koepke, J., Lecomte, C., Guillot, B., Jelsch, C., *et al.* (2013) Hydrogen atoms in protein structures: high-resolution X-ray diffraction structure of the DFPase. *BMC Res. Notes* **6**, 308

48. Chakraborti, S., and Bahnson, B. J. (2010) Crystal structure of human senescence marker protein 30: insights linking structural, enzymatic, and physiological functions. *Biochemistry* **49**, 3436–3444

49. Josse, D., Ebel, C., Stroebel, D., Fontaine, A., Borges, F., Echalier, A., *et al.* (2002) Oligomeric states of the detergent-solubilized human serum paraoxonase (PON1). *J. Biol. Chem.* **277**, 33386–33397

50. Grunkemeyer, T. J., Mata, D. G., Doddapaneni, K., Murali, S., and Magliery, T. J. (2018) Insights into the mechanism of paraoxonase-1: comparing the reactivity of the six-bladed beta-propeller hydrolases. *Biochemistry.* https://doi.org/10.1021/acs.biochem.8b01115

51. Le, Q. A., Kim, S., Chang, R., and Kim, Y. H. (2015) Insights into the lactonase mechanism of serum paraoxonase 1 (PON1): experimental and quantum mechanics/molecular mechanics (QM/MM) studies. *Journal Physical Chemistry. B* **119**, 9571–9585

52. Khersonsky, O., and Tawfik, D. S. (2006) The histidine 115-histidine 134 dyad mediates the lactonase activity of mammalian serum paraoxonases. *J. Biol. Chem.* **281**, 7649–7656

53. Larimer, F. W., Chain, P., Hauser, L., Lamerdin, J., Malfatti, S., Do, L., *et al.* (2004) Complete genome sequence of the metabolically versatile photosynthetic bacterium Rhodopseudomonas palustris. *Nat. Biotechnol.* **22**, 55–61

54. Kim, M.-K., and Harwood, C. S. (1991) Regulation of benzoate-CoA ligase in Rhodopseudomonas palustris. *FEMS Microbiol. Lett.* **83**, 199–203

55. McKinlay, J. B., and Harwood, C. S. (2010) Carbon dioxide fixation as a central redox cofactor recycling mechanism in bacteria. *Proc. Natl. Acad. Sci. U. S. A* **107**, 11669–11675

56. Rand, J. M., Pisithkul, T., Clark, R. L., Thiede, J. M., Mehrer, C. R., Agnew, D. E., *et al.* (2017) A metabolic pathway for catabolizing levulinic acid in bacteria. *Nat. Microbiol.* **2**, 1624–1634

57. Gall, D. L., Ralph, J., Donohue, T. J., and Noguera, D. R. (2014) A group of sequence-related sphingomonad enzymes catalyzes cleavage of beta-aryl ether linkages in lignin beta-guaiacyl and beta-syringyl ether dimers. *Environ. Sci. Technol.* **48**, 12454–12463

58. Novy, R., Drott, D., Yaeger, K., and Mierendorf, R. (2001) Overcoming the codon bias of *E. coli* for enhanced protein expression. *inNovations* **12**, 1–3

59. Studier, F. W. (2005) Protein production by auto-induction in high-density shaking cultures. *Protein Expr. Purif.* **41**, 207–234

60. Sreenath, H. K., Bingman, C. A., Buchan, B. W., Seder, K. D., Burns, B. T., Geetha, H. V., *et al.* (2005) Protocols for production of selenomethionine-labeled proteins in 2-L polyethylene terephthalate bottles using auto-induction medium. *Protein Expr. Purif.* **40**, 256–267

61. Suelter, C., and DeLuca, M. (1983) How to prevent losses of protein by adsorption to glass and plastic. *Anal. Biochem.* **135**, 112–119

62. Draganov, D. I., Stetson, P. L., Watson, C. E., Billecke, S. S., and La Du, B. N. (2000) Rabbit serum paraoxonase 3 (PON3) is a high density lipoprotein-associated lactonase and protects low density lipoprotein against oxidation. *J. Biol. Chem.* **275**, 33435–33442

63. Price, M. N., and Arkin, A. P. (2017) PaperBLAST: text mining papers for information about homologs. *mSystems* **2**, e00039-17

64. Madeira, F., Park, Y. M., Lee, J., Buso, N., Gur, T., Madhusoodanan, N., *et al.* (2019) The EMBL-EBI search and sequence analysis tools APIs in 2019. *Nucleic Acids Res.* **47**, W636–W641

65. Kozlov, A. M., Darriba, D., Flouri, T., Morel, B., and Stamatakis, A. (2019) RAxML-NG: a fast, scalable and user-friendly tool for maximum likelihood phylogenetic inference. *Bioinformatics* **35**, 4453–4455

66. Miller, M. A., Pfeiffer, W., and Schwartz, T., Creating the CIPRES Science Gateway for inference of large phylogenetic trees, In: *Proceedings of the Gateway Computing Environments Workshop (GCE)14 Nov 2010, New Orleans, LA*, 1–8.

67. Kabsch, W. (2010) XDS. *Acta Crystallogr. D Biol. Crystallogr.* **66**, 125–132

68. Diederichs, K. (2006) Some aspects of quantitative analysis and correction of radiation damage. *Acta Crystallogr. D Biol. Crystallogr.* **62**, 96–101

69. Liebschner, D., Afonine, P. V., Baker, M. L., Bunkóczi, G., Chen, V. B., Croll, T. I., *et al.* (2019) Macromolecular structure determination using X-rays, neutrons and electrons: recent developments in phenix. *Acta Crystallogr. D Struct. Biol.* **75**, 861–877

70. Afonine, P. V., Grosse-Kunstleve, R. W., Echols, N., Headd, J. J., Moriarty, N. W., Mustyakimov, M., *et al.* (2012) Towards automated crystallographic structure refinement with phenix.refine. *Acta Crystallogr. D Biol. Crystallogr.* **68**, 352–367

71. Emsley, P., Lohkamp, B., Scott, W. G., and Cowtan, K. (2010) Features and development of Coot. *Acta Crystallogr. D Biol. Crystallogr.* **66**, 486–501

72. Grosse-Kunstleve, R. W., and Adams, P. D. (2003) Substructure search procedures for macromolecular structures. *Acta Crystallogr. D Biol. Crystallogr.* **59**, 1966–1973

ASBMB

J. Biol. Chem. (2023) 299(1) 102782 **15**

73. Terwilliger, T. C., Adams, P. D., Read, R. J., McCoy, A. J., Moriarty, N. W., Grosse-Kunstleve, R. W., *et al.* (2009) Decision-making in structure solution using Bayesian estimates of map quality: the PHENIX AutoSol wizard. *Acta Crystallogr. D Biol. Crystallogr.* **65**, 582–601

74. Morris, R. J., Perrakis, A., and Lamzin, V. S. (2003) ARP/wARP and automatic interpretation of protein electron density maps. *Methods Enzymol.* **374**, 229–244

75. Moriarty, N. W., Grosse-Kunstleve, R. W., and Adams, P. D. (2009) Electronic Ligand Builder and Optimization Workbench (eLBOW): a tool for ligand coordinate and restraint generation. *Acta Crystallogr. D Biol. Crystallogr.* **65**, 1074–1080

76. Smart, O. S., Womack, T. O., Sharff, A., Flensburg, C., Keller, P., Paciorek, W., *et al.* (2011) *Grade, Version 1.2.20,* Global Phasing Ltd, Cambridge, United Kingdom

77. Bruno, I. J., Cole, J. C., Kessler, M., Luo, J., Motherwell, W. S., Purkis, L. H., *et al.* (2004) Retrieval of crystallographically-derived molecular geometry information. *J. Chem. Inf. Comput. Sci.* **44**, 2133–2144

78. Terwilliger, T. C., Klei, H., Adams, P. D., Moriarty, N. W., and Cohn, J. D. (2006) Automated ligand fitting by core-fragment fitting and extension into density. *Acta Crystallogr. D Biol. Crystallogr.* **62**, 915–922

79. Watson, C., Draganov, D., Billecke, S., Bisgaier, C., and La Du, B. (2001) Rabbits possess a serum paraoxonase polymorphism similar to the human Q192R. *Pharmacogenetics* **11**, 123–134

80. Ahmed, H., Ettema, T. J. G., Tjaden, B., Geerling, A. C. M., van der Oost, J., and Siebers, B. (2005) The semi-phosphorylative Entner-Doudoroff pathway in hyperthermophilic archaea: A re-evaluation. *Biochem. J.* **390**, 529–540

81. Price, M. N., Wetmore, K. M., Waters, R. J., Callaghan, M., Ray, J., Liu, H., *et al.* (2018) Mutant phenotypes for thousands of bacterial genes of unknown function. *Nature* **557**, 503–509

82. Price, M. N., Ray, J., Iavarone, A. T., Carlson, H. K., Ryan, E. M., Malmstrom, R. R., *et al.* (2019) Oxidative pathways of deoxyribose and deoxyribonate catabolism. *mSystems* **4**, e00297-18

83. Watanabe, S., Shimada, N., Tajima, K., Kodaki, T., and Makino, K. (2006) Identification and characterization of l-arabonate dehydratase, l-2-keto-3-deoxyarabonate dehydratase, and l-arabinolactonase involved in an alternative pathway of l-arabinose metabolism: novel evolutionary insight into sugar metabolism. *J. Biol. Chem.* **281**, 33521–33536

84. Letunic, I., and Bork, P. (2021) Interactive tree of Life (iTOL) v5: an online tool for phylogenetic tree display and annotation. *Nucleic Acids Res.* **9**, W293–W296